

Rapid solidification in thermal spray deposition: Microstructure and modelling

GUO-XIANG WANG¹, V PRASAD² and S SAMPATH²

¹Department of Mechanical Engineering, The University of Akron, Akron, OH 44325-3903, USA

²Center for Thermal Spray Research, College of Engineering and Applied Sciences, State University of New York at Stony Brook, Stony Brook, NY 11794-2200, USA

e-mail: gwang@uakron.edu

Abstract. Mechanical, thermal, and adhesive properties of thermal spray coatings are primarily determined by the phase and microstructure of single splats, which ultimately depend on rapid solidification of each splat and on the interactions between the splats and between the splat and the substrate. Significant efforts are being made to develop a better understanding of the physical mechanisms underlying these phenomena. This paper reviews a series of work in the area of mathematical modelling of phase and microstructure formation during the rapid solidification of single splats and coatings. The model development has been complimented by special experiments. Conditions under which planar interface solidification occurs, columnar cellular or dendritic growth takes place, or banded structure forms, have been identified. A microstructure map can therefore be built using the model presented here. The process parameters that promote crystalline nucleation and grain structure formation can be isolated and the effect of interfacial heat transfer, splat substrate temperature difference, and substrate melting and resolidification can be examined using the model. The model predictions agree qualitatively well with the experimental data for alumina, yttria, partially-stabilized zirconia, and molybdenum.

Keywords. Thermal spray coatings; splats; rapid solidification.

1. Introduction

Thermal spray deposition is a growing industrial process that produces engineered surfaces with highly desired mechanical and thermal properties (Sampath & Herman 1996). In thermal spray deposition, the stock powders are fed into a plasma or combustion flame where the powders heat up, melt, and accelerate. High-speed molten droplets then impact on a solid (substrate) surface and spread to form pancake-shaped splats. Millions of such

^{*}Corresponding author

splats pile up together to form a coating. Because of very high velocities, several hundred metres per second, very thin splats are formed, that experience rapid solidification due to extremely high rate of heat transfer (Jacobson & McKittrick 1994; Sampath & Hernan 1996; Wang G-X & Prasad 2000).

The plasma spraying process was first developed in an empirical manner, mainly by trial and error variations of input parameters, such as operating current or the gas feed rate, that determine the quality of the coating indirectly. Since the trial and error experiments are expensive and time-consuming and the empirical optimization is approaching its limits, significant research efforts are being devoted to direct evaluation of the process parameters and their impact, for better understanding of the fundamental phenomena and their influence on the coating quality. Since the coating is built upon small splats, special attention is being paid to characterize single splat formation and microstructure development. In particular, the Center for Thermal Spray Research at Stony Brook is conducting an extensive investigation to quantify and predict the formation of phase and microstructure of various materials during thermal spray deposition. Both experimental and theoretical approaches have been adopted that compliment each other. The experimental studies have documented the existence of various phases and microstructural forms in the plasma-sprayed splats and coatings (e.g., Goswami *et al* 1999, Jiang *et al* 1999, 2000, Sampath *et al* 1999). Also, models have been developed to explain the physical mechanisms of the formation of these phases and microstructures (e.g., Wang G-X *et al* 2000). A brief review of this research is presented here.

2. Physical mechanisms of microstructure formation in a sprayed splat

In a thermal spray, when a molten droplet impacts on the substrate, or a previously deposited layer, it spreads and forms a thin, pancake-shaped liquid splat with the splat diameter much larger than the splat thickness (figure 1). The final microstructure of the subsequently solidified splat results from the competition between the crystalline nucleation and growth. In most cases, heterogeneous nucleation takes place on the lower

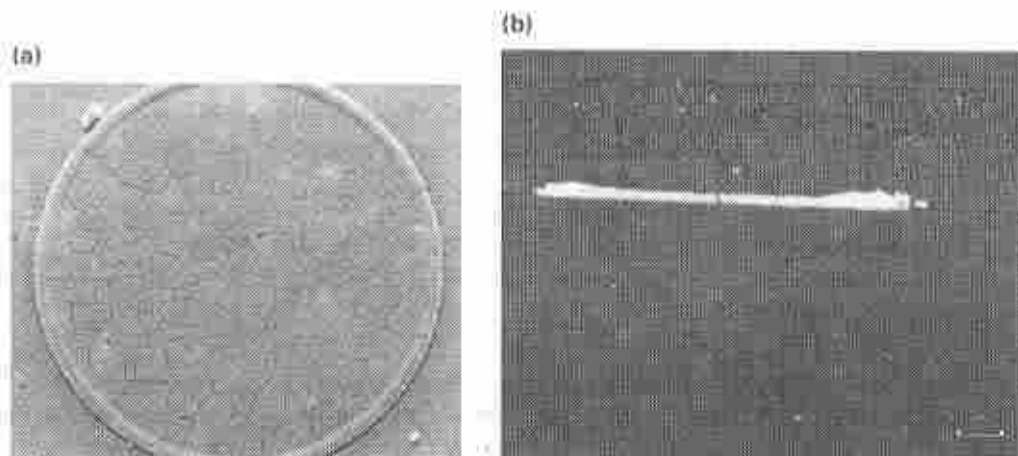


Figure 1. (a) A yttria stabilized zirconia splat sprayed on a hot steel substrate; the splat diameter is about 150 μm . (b) The cross-section of a molybdenum splat sprayed on a hot substrate (Jiang *et al* 1999).

side of the splat where the melt is in contact with the colder substrate, or the previously deposited layer. The crystalline nuclei then grow into the undercooled melt in all directions and quickly form a solid shell covering the substrate surface, followed by columnar growth normal to the substrate surface. Occasionally, heterogeneous nucleation may also occur within the bulk liquid due to the existence of the impurities in the melt, which leads to equiaxed grains in the splat. In the case of surface nucleation, columnar grains grow into the top surface with a uniform distribution of the solute elements provided a stable planar interface exists throughout the solidification process. Otherwise, cells may develop within a grain and alloy elements be segregated along the cell surface. Because of the very small thickness of the splat and extremely high solidification rate, very little time is available for cells to develop into full dendrites.

Small splat thickness and high rates of heat transfer and melt cooling lead to rapid solidification in thermally sprayed splats and coatings, that is characterized by the formation of various metastable phases and extremely fine grain structures (Sampath & Herman 1996). For example, metastable γ phase is found in a sprayed Al_2O_3 splat, instead of the stable α phase (McPherson 1980). In the coatings of eutectic composition of Ni-Cr, single Ni-Cr solution has been observed, instead of a eutectic phase (Sampath *et al* 1993). When the melt is undercooled, the growth of crystalline nuclei occurs under non-equilibrium conditions with the solid/liquid interface temperature much different from the equilibrium freezing temperature. Such non-equilibrium solidification further adds to the formation of new and complex microstructures, compared to the solidification under local equilibrium conditions (Kurz & Fisher 1989).

Rapid solidification in sprayed splats is quite different from that in atomized droplets and in laser surface melting. In an atomized droplet (Levy & Mehrabian 1982; Kim *et al* 1994), the melt may be undercooled significantly below the equilibrium temperature before the crystalline phase is formed. As a result, the crystalline phase grows into an undercooled melt with very little external heat transfer. Solidification is then characterized by the free growth of solid dendrites into an undercooled melt with negative temperature gradients ahead of the dendrites. On the other hand, the crystalline phase in laser surface melting grows from the unmelted parent phase with melt undercooling developed slowly at the interface due to a high rate of solidification. Crystalline growth is then constrained by a strong positive temperature gradient in the solid and a small positive temperature gradient in the liquid, leading to a pure columnar structure (Wang G-X & Matthys 1996a). In a sprayed splat, the crystalline nuclei usually form on the bottom surface of the melt that is in contact with the substrate, or the previous deposit, which is significantly undercooled. Therefore, crystalline growth in the beginning is similar to the free growth in an undercooled droplet. The difference is that in a sprayed splat, a large temperature gradient exists in the solidified solid because of the high rate of heat transfer from the splat to the substrate. As the recalescence approaches its end, the melt may be heated up and the melt undercooling may disappear, leading to transition to a constrained growth as in laser surface melting. Such variations in thermal conditions during the solidification of a sprayed splat lead to the formation of complex microstructures. They also make the mathematical modelling of splat solidification very challenging.

3. Model development for splat solidification and microstructure formation

In thermal spray deposition, as a molten droplet impinges on the substrate with high velocity, the melt deforms and spreads to form a liquid splat. The liquid splat then quickly

solidifies. Final microstructure formation depends on the initial splat formation that determines the splat thickness and geometry integrity, and subsequent nucleation and solidification. Melt spreading and deformation involve complex fluid dynamics issues that have been a topic of several recent studies (Mostaghimi *et al* 1999; Zhang 1999). However, as a first approximation, one can treat melt spreading and splat solidification separately, since the time-scale for melt spreading and liquid splat formation is generally much smaller than that for splat solidification (Trapaga & Szekely 1991).

Splat solidification and microstructure formation in a sprayed splat involves complex physical principles including rapid heat and mass transport, kinetics of crystalline nucleation, non-equilibrium crystalline growth, and dynamic change in solidification morphology. Traditionally, a solidification process has been treated as a moving boundary problem with the latent heat transfer and segregation/mass transfer only as the primary concern. Recently, efforts have been made to incorporate solidification kinetics into these models to simulate microstructure formation (Rappaz 1989; Beckermann & Wang 1995; Wang G-X & Prasad 2000).

The complexity of modelling microstructure formation in a sprayed splat arises from the treatment of complex crystalline nucleation kinetics and subsequent crystalline growth morphologies. The present authors and their co-workers have developed a simple model that can be used to simulate microstructure formation in a sprayed splat (Robert *et al* 1998a; Wang G-X & Matthys 1992, 1993; Wang G-X *et al* 2000). The models solve one-dimensional heat and mass diffusion problems in both splat and substrate, with the initial and moving boundary conditions dictated by the phenomenological models of crystalline nucleation and growth kinetics. The simplification to a one-dimensional problem is justified by the splat thickness being much smaller than its diameter. Several issues that were paid special attention in the model development include: (1) crystalline nucleation and phase formation, (2) non-equilibrium crystalline growth kinetics with melt undercooling, (3) planar interface stability, and (4) solidification morphology including cellular or dendritic growth. By introducing kinetic physics in the model, it is possible to ultimately correlate the formation of phase and microstructure in a splat with the processing conditions. The model can also be used to construct microstructure maps that can be used to tailor the microstructure formation in a given process. A brief description of the model is presented below.

3.1. Planar interface solidification

When the solidification velocity is larger than the absolute stability velocity, a planar interface exists during solidification (figure 2a). The governing equations for planar interface solidification of a binary alloy system can be written as:

$$\rho_j C_j v_j \frac{\partial T_j}{\partial t} = \frac{\partial}{\partial y} \left(k_j \frac{\partial T_j}{\partial y} \right), \quad (1)$$

$$\frac{\partial C_j}{\partial t} = \frac{\partial}{\partial y} \left(D_j \frac{\partial C_j}{\partial y} \right), \quad (2)$$

where subscript j stands for the substrate, solidified material, or melt. (No mass diffusion equation needs to be solved in the substrate.) For pure materials, solute diffusion equation (2) does not need to be considered.

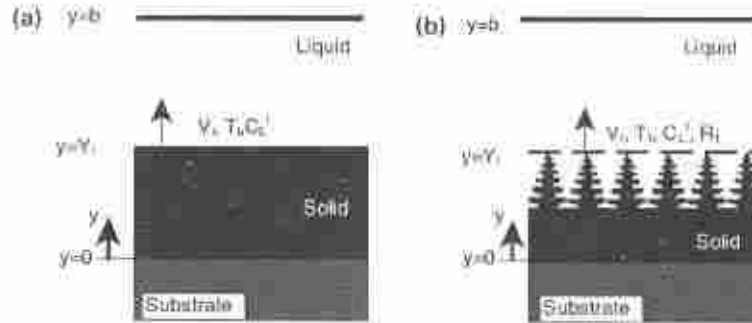


Figure 2. Schematic of solidification patterns in columnar growth: planar interface (a) and dendritic (b) solidification.

There exist four unknown parameters at the moving solid/liquid interface for such a moving boundary problem: interface velocity, V_i ; interface temperature, T_i ; and solute concentrations of liquid (C_L^i) and solid (C_S^i). The conservation laws for energy and mass provide the conditions:

$$\rho_L V_i L = K_S \left. \frac{\partial T_S}{\partial y} \right|_i - K_L \left. \frac{\partial T_L}{\partial y} \right|_i, \quad (3)$$

$$(C_L^i - C_S^i) V_i = D_S \left. \frac{\partial C_S}{\partial y} \right|_i - D_L \left. \frac{\partial C_L}{\partial y} \right|_i, \quad (4)$$

where L is the latent heat of fusion and ρ_L is the liquid density. Two other conditions, called response functions by Baker & Cahn (1971), can be obtained from the consideration of non-equilibrium crystalline growth kinetics of alloys. These, in a general form, can be presented as:

$$\begin{aligned} f_1(V_i, T_i, C_L^i, C_S^i) &= 0, \\ f_2(V_i, T_i, C_L^i, C_S^i) &= 0. \end{aligned} \quad (5)$$

For a dilute binary alloy, they can be written as (Aziz 1982; Boettinger & Coriell 1986; Wang G-X & Mathys 1996a):

$$T_i = T_m + m_L C_L^i - V_i / \mu_k, \quad (6)$$

$$k = C_S^i / C_L^i = (k_e + V_i / V_D) / (1 + V_i / V_D), \quad (7)$$

where T_m is the equilibrium melting temperature of the solvent, m_L is the slope of the non-equilibrium liquidus curve, μ_k is the linear kinetics coefficient, k is the non-equilibrium partition coefficient, and V_D is the characteristic diffusion velocity of atoms at the interface.

If the equilibrium liquidus and solidus curves are straight lines, the non-equilibrium liquidus slope m_L can be calculated from (Boettinger & Coriell 1986),

$$m_L = m_L^e [1 + (k_e - k + k \ln(k/k_e)) / (1 - k_e)], \quad (8)$$

where m_L^e is the equilibrium liquidus slope and k_e is the equilibrium partition coefficient. It should be noted that the modification of the liquidus slope requires that, as the non-

equilibrium partition coefficient approaches unity, the interface temperature should approach T_0 , the temperature at which the solid and liquid phases for identical compositions have equal free energies.

3.2 Columnar cellular or dendritic solidification

Columnar cellular or dendritic solidification involves complex shapes of the solid/melt interface, and explicit tracking of this interface is not an easy task, nor is it practical for engineering modeling. Traditionally, these problems have been treated by considering the solid/liquid region as a solid/liquid mixture or a porous medium (i.e. a mushy zone) with uniform effective properties (Clyne 1982; Beckermann & Wang 1995). This allows one to avoid the complexity of the solid/melt interface geometries. If convection in the melt is neglected, no macroscopic segregation of the constituents needs to be considered, which leads to a macroscopic heat transfer equation as:

$$\rho_j C_{pj} \frac{\partial T_j}{\partial t} = \frac{\partial}{\partial y} \left(K_j \frac{\partial T_j}{\partial y} \right) + \rho_c L \frac{\partial f_s}{\partial t}, \quad (9)$$

where solidification fraction $f_s = 0$ in the liquid, $f_s = 1$ in the solid and $f_s = f(T, C, y, t)$ in the mushy zone. For alloy solidification with localized equilibrium conditions, various models have been developed for the functional form of f_s from microsegregation analysis (Bartle 1992). Complex relationships for f_s have also been derived recently by taking into account the effect of finite solute diffusion and non-equilibrium solidification kinetics (Giovanola & Kurz 1990; Wang G-X *et al* 1998).

If the melt is significantly undercooled, then special treatment for the tip fronts of the growing cells or dendrites are needed. Following Flood & Hunt (1987), an artificial interface that envelops the tips (figure 2b) of cells or dendrites can be defined with the interface moving at the same speed as the tips. Thermodynamics and kinetics considerations of crystalline growth require that the temperature at this interface (i.e., the tips) must follow the following relationship (Trivedi & Kurz 1994):

$$T_t = T_m + m_L C_t^* - 2\Gamma/R_t - V_t/lk, \quad (10)$$

where sub- and super-script t stand for the tip of the cells and dendrites. The solute concentration at the tip depends on the local solute diffusion around the tip, and can be approximated by Ivantsov's steady state solution for a paraboloid dendrite:

$$C_t^* = C_0 / (1 - (1 - k)Iv(P_c)). \quad (11)$$

The tip radius can be determined based on the "marginal" stability condition, as suggested by Trivedi & Kurz (1994):

$$R_t = (\Gamma/\sigma^*)^{1/2} (m_L G_C \xi_C - (K_L G_L \xi_L + K_S G_S \xi_S) / (K_L + K_S))^{1/2}, \quad (12)$$

where the solute gradient G_C at the tip can be calculated from the solute balance at the tip:

$$G_C = -V_t C_t^* (1 - k) / D_L. \quad (13)$$

The other two macroscopic variables, G_L and G_S , are the temperature gradients at the melt/tip interface, in the melt and solid regions respectively. Equations (10)–(13) constitute a self-consistent dendrite tip growth model. For given values of G_L and G_S , the model can be used to calculate all the tip parameters. The two temperature gradients are the parameters that introduce the effect of macroscopic thermal transport on microscale dendrite tip growth. Theoretically, the microscopic dendrite tip model provides the necessary conditions for the moving tip/melt interface that can be combined with the macroscopic heat equation to calculate G_L and G_S . However, the macroscopic temperature gradients must be specified in order to solve the dendrite model. Therefore, an integrated treatment must be adopted in which both micro and macroscopic equations are solved simultaneously. In addition, since the interface stability criterion is implicitly built into the above dendritic growth model through the term in the square root of (12), the model can also detect the change of the solidification morphology from dendritic to planar, or vice versa. For example, if the term in the square root in (12) becomes negative, a transition from dendritic growth to planar growth occurs (Trivedi & Kurz 1994; Wang G-X *et al* 2000a).

The present model is different from the ones that exist in the literature for rapid solidification. All the existing models employ a prescribed interface temperature-velocity relationship, derived from the steady-state dendritic growth model with a special thermal condition (Flood & Hunt 1987; Granasy & Ludwig 1992; Kim *et al* 1994). Such a treatment implicitly pre-assumes the solidification morphology and is therefore not able to deal with situations where the solidification morphology can change. The present model, on the other hand, does not make such an implicit assumption and can treat the transition from a planar to cellular/dendritic solidification that is considered critical for predicting microstructure formation.

3.3 Crystalline nucleation and grain structure formation

Most of the existing rapid solidification models simplify the treatment of nucleation by arbitrarily assigning a nucleation temperature below the equilibrium temperature because of the uncertainty of the nucleation kinetics (Levi & Mehrabian 1982; Wang G-X & Mathys 1992). The effect of nucleation temperature on crystalline growth can then be investigated by systematically changing the preset nucleation temperature. Obviously, such a simplified treatment of nucleation does not yield the necessary information to predict grain development in the splat.

Recently, efforts have been made to build models that can simulate the grain structure formation within a splat, by introducing the classical nucleation theory into the existing solidification model. These models consider a heterogeneous nucleation process occurring at the substrate surface. Nucleation kinetics equations are obtained from the classical nucleation theory assuming a steady-state nucleation process. The catalytic effect of the substrate surface is considered by a contact angle θ between the nucleus and the catalytic surface. Even though it is well-known that the contact angle plays a dominant role in the nucleation process and the selection of the crystalline phase, very little information is available on the value of θ for different materials. Nevertheless, one can set up the nucleation model for grain structure development by treating the contact angle as a free parameter. Efforts have also been made to determine indirectly the possible values of θ by comparing the crystalline grain density predicted by the model and the density deduced

from the splat observation. The nucleation model used for splat solidification is deduced below (Levi 1988; Vardelle *et al* 1997; Robert *et al* 1998).

The total number of nuclei, N , formed at any time instant, t , can be calculated from:

$$N = \int_{t_m}^t I(T) dt, \quad (14)$$

where t_m corresponds to the time when the liquid temperature reaches T_m , and I is the rate of nucleus formation. Assuming a steady-state nucleation process, the rate of nucleation I can be calculated from the classical nucleation theory (Levi 1988; Feuerbacher 1989)

$$I = N_f \frac{\kappa_B T}{h} \Gamma_z \exp\left(-\frac{\Delta G_d}{\kappa_B T}\right) \exp\left(-\frac{\Delta G_c f(\theta)}{\kappa_B T}\right), \quad (15)$$

where ΔG_d is the activation energy for interatomic diffusion in the liquid, κ_B is the Boltzmann constant, h is Planck's constant, and $\Gamma_z = [\Delta G_c / (3\pi\kappa_B T)]^{1/2}$ is known as the Zeldovich factor. In (15), $f(\theta)$ represents a function that represents the magnitude of the effect of the surface on the lowering of the activation energy barrier for nucleation, i.e.,

$$\Delta G_c^{het} = \Delta G_c f(\theta) = \Delta G_c^{hom} (2 - 3 \cos \theta + \cos^3 \theta) / 4, \quad (16)$$

where ΔG_c^{het} and ΔG_c are the nucleation barriers for heterogeneous and homogeneous nucleation respectively. Over the variation in θ ranging from complete wetting to non-wetting, $f(\theta)$ varies from 0 to 1. This change in nucleation barrier has significant influence on the nucleation rate (Clyne 1984; Vardelle *et al* 1997).

The atoms involved in the nucleation process will be the ones that are in direct contact with the foreign surface(s) where the surface catalytic effect is strong, i.e., the substrate surface in the present case. Hence the numbers of atoms that are involved in nucleation can be approximated from

$$N_i = a_0 A_j N_a / \Omega, \quad (17)$$

where a_0 is the molecular diameter, N_a is the Avogadro's number, Ω is the molar volume of the material, and A_j is the surface area of the melt in contact with the substrate.

The nucleation starts when $N = 1$ with the nucleation temperature, T_N , defined as the temperature of the melt when the first nucleus appears. After the onset of nucleation, the formed nuclei are assumed to grow in all directions by attachment of the surrounding atoms in the melt, while other nuclei can appear on the substrate surface. Note that the nuclei are assumed to have a spherical-cap shape. For pure materials, the interface velocity of the growing nuclei can be calculated from the linear kinetic equation:

$$V_i = \mu_k (T_m - T_i), \quad (18)$$

In numerical calculations, the interface temperature T_i of the nuclei is approximated by the nodal temperature of the control volume where the nucleation occurs.

The latent heat released due to the growth of already nucleated crystals heats up the undercooled melt and thus changes the melt temperature. This effect is also taken into

account by a source term in the energy equation for the control volume in which the nucleation takes place:

$$Q_j = \rho_l L (\partial v_j / \partial t), \quad (19)$$

where v_j is the total volume of nuclei.

When solid nuclei cover 67% of the bottom surface of the splat in contact with the substrate, nucleation is assumed completed. It corresponds to the portion of the surface covered by the "closely-packed" circles. The solidification of the splat then takes place with a planar liquid/solid interface. The initial thickness, \bar{b} , of the solidified layer is calculated as the average of the various grain thicknesses, b_i :

$$\bar{b} = \left(\sum N_i b_i \right) / N. \quad (20)$$

For materials with metastable phases, the nucleation of those metastable phases can also be incorporated into the model using the same set of nucleation rate equations but with different nucleation barriers and contact angles. For example, for the alumina system, the model introduces a competitive nucleation process among three possible phases: stable α phase, and two metastable phases, δ and γ (Robert *et al* 1998a). The final preferred phase that nucleates will correspond to the first nucleus appearing among the three different kinds in competition.

3.4 Interfacial heat transfer, substrate melting and resolidification

One of the parameters that is critical in splat solidification is the thermal contact resistance between the splat and the substrate or the previous deposit. It is found that the thermal contact resistance can dictate the rate of heat transfer and splat microstructure formation. In most models, the thermal contact resistance is represented quantitatively by a thermal conductance, referred to as interfacial heat transfer coefficient, h . Since the interface contact condition between the splat and the substrate changes from the initial liquid/solid to solid/solid condition as the splat solidifies, the value of h is expected to be a strong function of time. However, since solidification takes place very fast, it is extremely difficult to measure the variation of h during the process. Instead, an average value of h is used throughout the entire solidification process. Only limited data are available on the interfacial heat transfer coefficient for rapid solidification (Moreau *et al* 1992; Wang G-X & Matthys 1996b). Wang G-X & Matthys (1996c) have presented a survey of the values of h suitable for rapid solidification processes including thermal spray deposition. It is estimated that the average value of h for a sprayed liquid splat on a substrate can range from 10^5 to 10^8 W/m²K.

When a high-melting point metal droplet impinges on a substrate, the high intensity of heat can lead to the melting of the substrate surface (Jiang *et al* 1999; Goswami 1999, unpublished results). The melting of a thin layer of substrate may lead to a strong bond between the coating layer and the substrate due to physical/chemical-metallurgical interactions at the interface. Experimental studies confirm that the interface interactions between the high melting point coating and the substrate are quite complex, and are significantly affected by the powder and substrate materials, their physical properties, and the thermal state of the droplets upon impacting. Substrate melting and resolidification have also been incorporated into the model (Wang S-P *et al* 1998, 1999). Operational maps for the onset of substrate melting have been developed and maximum melting depth in the substrate has been predicted.

4. Characteristics of rapid solidification in a splat

The solidification characteristics of a sprayed splat have been extensively studied by Wang G-X *et al.* (2000a) using the above model. They have considered a 5- μm thick molten Al-4.5wt%Cu splat quenched on a copper substrate, with the initial melt being at 983.6 K and the substrate at 300 K. The nucleation temperature, T_N , and the interfacial heat transfer coefficient, h , are treated as free parameters. To avoid the complexity of the mushy zone and following Kim *et al.* (1994), the dendrite region is considered to be thin and the latent heat is assumed to be released only at the tip/melt interface. This assumption can be easily relaxed by introducing a microsegregation model.

Figure 3a shows typical predictions for dendritic tip radius when $h = 10^7 \text{ W/m}^2\text{K}$ and the melt undercooling varies from 50 K to 250 K. In all cases, the initial tip radius is small, 0.15 μm for 250 K and about 0.32 μm for 50 K. As the solidification progresses, the tip radius increases with the rate being a strong function of the melt undercooling. A larger initial melt undercooling results in a lower rate of increase in the tip radius. Eventually, the tip radius becomes so large that dendritic growth becomes unstable and planar interface solidification follows. The extent to which dendritic solidification can occur strongly depends on the initial melt undercooling.

The corresponding velocity of the interface, for both dendritic and planar interface growth, is shown in figure 3b. Variation of the interface velocity as shown in this figure is very similar to that observed in the case of planar interface solidification of pure metals and binary alloys (Wang G-X & Mathys 1991). A high interface velocity is achieved at the beginning of the solidification because of a large melt undercooling. Recalescence then follows due to the heating of the undercooled melt by the release of latent heat. Eventually, the kinetic effects fade away as the melt undercooling diminishes, and the solidification is controlled by the rate of heat transfer as illustrated by an identical interface velocity for varying initial melt undercooling.

One interesting phenomenon revealed by the model is the oscillatory behaviour of planar interface solidification when h is in the range of $2 \times 10^6 < h \leq 8 \times 10^6 \text{ W/m}^2\text{K}$, as shown in figure 4 for $h = 6 \times 10^6 \text{ W/m}^2\text{K}$. The transition from dendritic to planar interface solidification takes place at about 2.2 μm location. A small perturbation occurs at this point due to transition, but is stabilized immediately and a stable planar interface growth continues until about 2.6 μm where a small oscillation is observed first which then quickly develops into a large amplitude oscillation. The oscillatory behaviour (almost identical amplitudes and frequencies) is independent of the mesh size and is considered to be a real physical phenomenon. Such oscillatory solidification leads to the formation of a solute band, i.e., periodic variation of solute distribution. For the conditions considered here, the solute concentration in the solid varies from a minimum of 4.12 wt% to a maximum of 6.0 wt% with a maximum bandwidth of about 0.19 μm under the present condition. The appearance of such a solute band agrees well with the banded structure theory (Caffard *et al.* 1992; Kurma & Sarkissian 1993).

The most important feature of the model is that it can help in constructing a microstructure map for an alloy splat quenched on a cold substrate. To demonstrate this, Wang G-X *et al.* (2000a) have chosen the interfacial heat transfer coefficient, h , and initial melt undercooling at nucleation, $T_L - T_N$, as two controlling process parameters, and have generated a microstructure-process map as shown in figure 5. As one can see, different structures are predicted for different combinations of these two variables. For the case with a high h and a large $T_L - T_N$, the splat is a two-layer structure: a dendritic structure in the

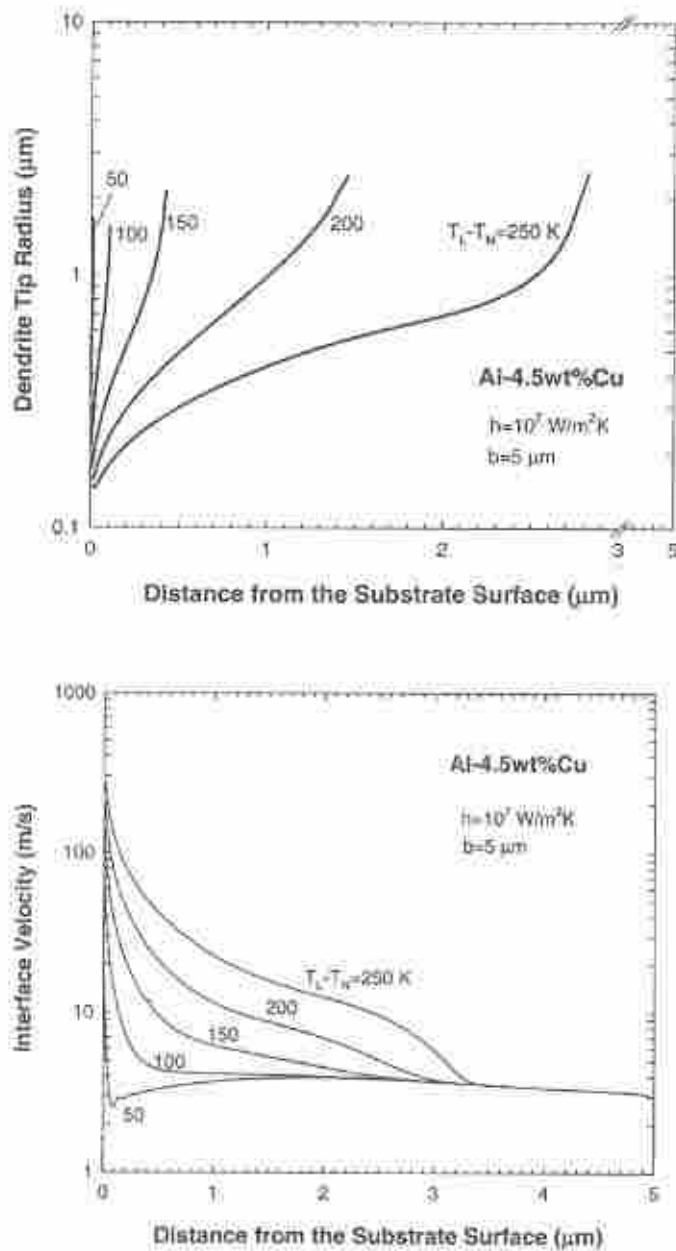


Figure 3. Effect of the melt undercooling on microstructure formation in an Al-4.5wt% Cu alloy splat quenched on a copper substrate: (a) the dendrite tip radius, and (b) the interface velocity (Wang G-X *et al* 2000a)

region close to the substrate followed by a planar interface growth region. For very low values of h , the entire splat is dendritic. In this case, if melt undercooling is large, large thermal dendrites will be developed in the region close to the substrate followed by small size solutal dendrites. However, if the melt undercooling is small, only solutal dendrites will exist. Banded thermal and solutal dendrite structures may also develop when transition from thermal dendritic growth to solutal dendritic growth occurs in the case of an intermediate melt undercooling.

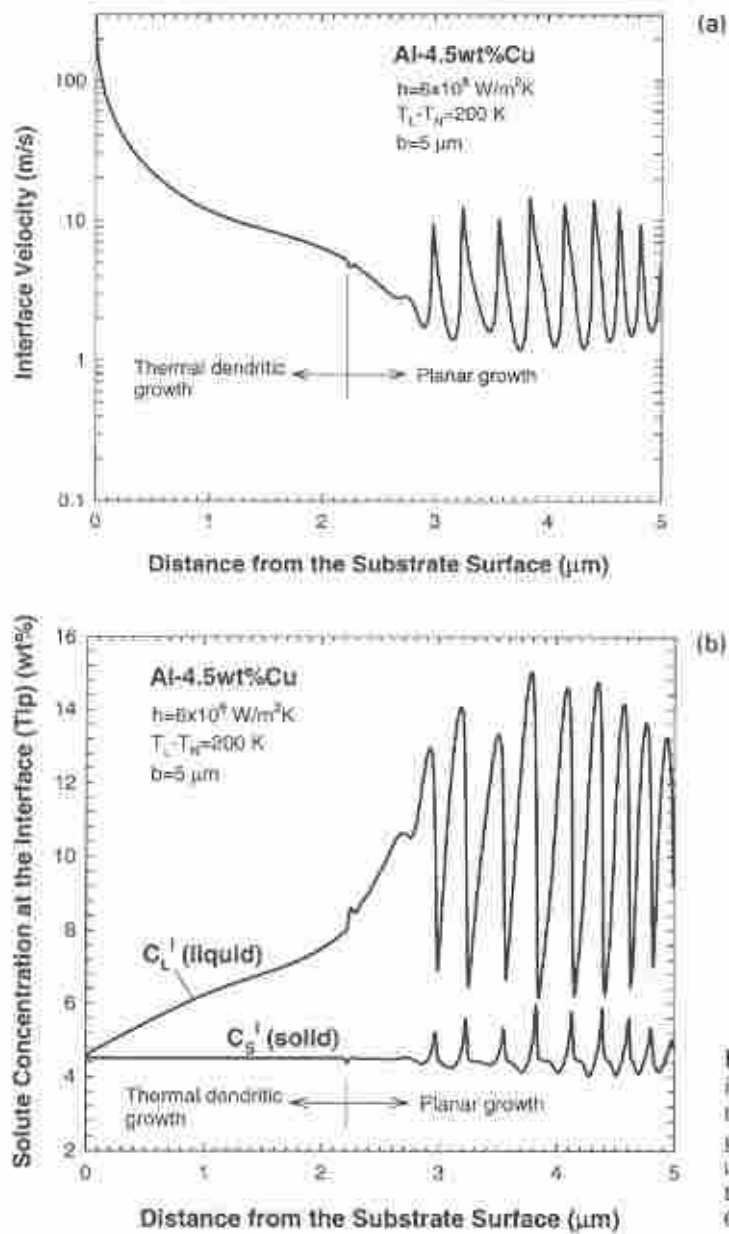


Figure 4. Oscillatory planar interface solidification after transition from the dendritic growth: (a) interface velocity, and (b) solute concentration in the solid at the interface (Wang G-X *et al* 2000a)

5. Applications of the model to microstructure formation in single splats and coatings

5.1 Alumina system

Alumina (Al_2O_3) based coatings are widely used in various industries including the automotive, steel, paper, and electrical power industries because of their resistance to abrasion, wear, corrosion, oxidation, thermal shock and high temperature (McPherson

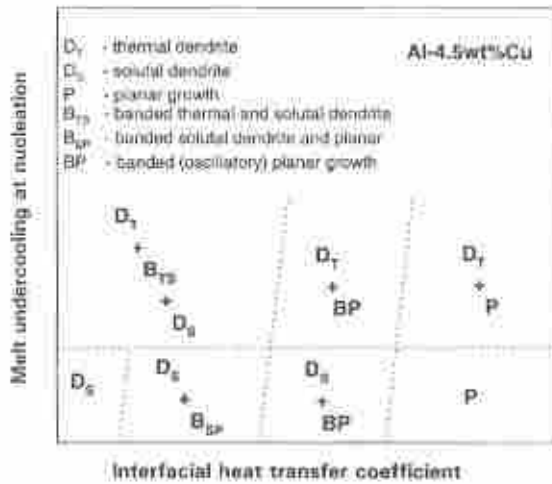


Figure 5. Schematic of a microstructure map for Al-4.5wt% Cu splat quenched on a copper substrate. Multiple layer structures with bands exist (Wang G-X *et al* 2000a).

1980; Gansert 1996). Extensive studies have been conducted to characterize and improve these coatings. Because alumina splats solidify under rapid solidification conditions, metastable γ phase is formed in the sprayed coatings, instead of the stable α phase. The physical properties of γ -Al₂O₃ are, however, generally inferior to those of α -Al₂O₃, and therefore it is important to be able to control the crystalline structure of the alumina deposits. Although it has long been realized that the nucleation kinetics of various crystalline phases determine the ultimate phase formation in the alumina system, modelling of crystalline nucleation and solidification in a thermally sprayed alumina splat and coatings was not possible until recently (Robert *et al* 1998a).

Robert *et al* (1998a) have used the nucleation model described above to study the grain structure development of an alumina splat of 1 μ m thickness and 100 μ m diameter at a uniform temperature of 3000 K quenched on a steel substrate. Figure 6 shows typical results for nucleation temperature as a function of the contact angle for the interfacial heat transfer coefficient of 10⁸ W/m²-K. It is evident that a large contact angle leads to a low nucleation temperature, i.e., large melt undercooling. Figure 6 also shows the effect of contact angle on phase selection under the condition that the surface has the same effect on

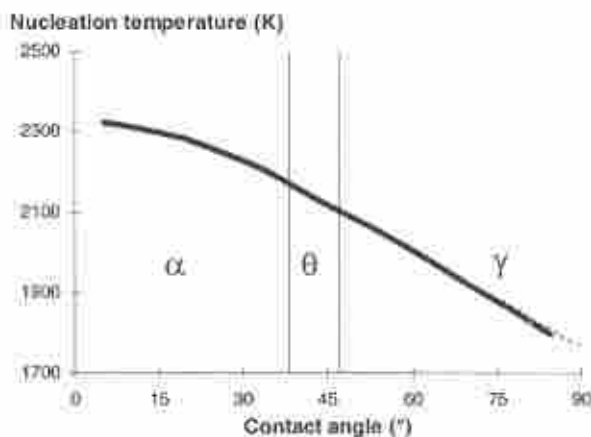


Figure 6. Nucleation temperature as a function of contact angle for three phases when an alumina splat is quenched on a steel substrate with an initial substrate temperature of 573 K. (The two vertical lines are the locations of transition from one phase selected over the other.) (Robert *et al* 1998a.)

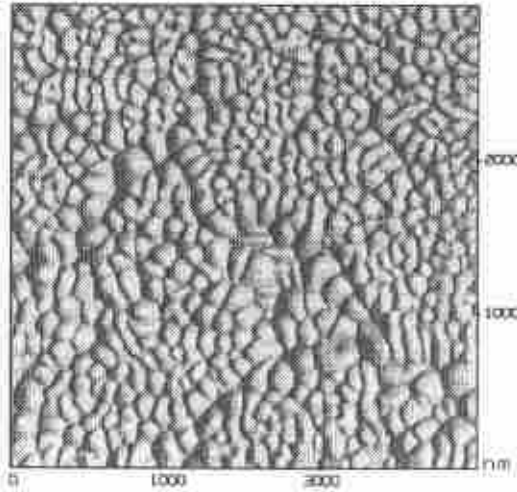


Figure 7. AFM picture of an alumina splat on a γ -alumina substrate preheated at 573 K (Robert *et al* 1998a).

three phases. As shown in this figure, the stable α phase nucleates at a higher nucleation temperature when the contact angle is small ($\theta < 37^\circ$), which implies a strong surface catalytic effect on nucleation. If the surface catalytic effect is weak, i.e., for a large contact angle, the metastable γ phase is nucleated at a low nucleation temperature with large melt undercooling. The metastable δ phase appears when the contact angle has a value between 37° and 48° .

Since the grain density and nucleation temperature depend strongly on the contact angle, its value must be chosen carefully for the model to be realistic. Unfortunately, no data is currently available in the literature. An attempt to estimate θ was made by Robert *et al* (1998a) by comparing the predicted and measured values of grain density and average grain size with the assumption that each nucleus grows into a grain, an assumption probably realistic for an extremely thin splat and fast rate of solidification. The grain density was obtained from a statistical analysis of the atomic force microscopy (AFM) pictures of the splat top surface as shown in figure 7 for an alumina splat collected on a γ -alumina substrate. The substrates were heated to 573 K before spraying. Figure 8 shows the comparison between experimental and predicted grain size distributions and it is

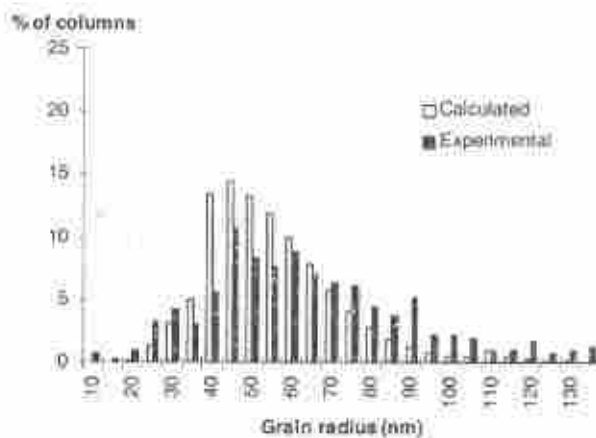


Figure 8. Comparison between the calculated and experimental grain size distributions for an alumina splat quenched on a γ - Al_2O_3 substrate at 573 K. The contact angle is taken as 66° (Robert *et al* 1998a).

evident that good agreement can be achieved if an appropriate value of θ is used. A slightly higher number of large grains in figure 8 than predicted by the model is probably due to the grain coarsening that is not included in the model. Robert *et al* (1998a) have examined several alumina splats sprayed over different substrate materials maintained at 573 K, and found that the contact angle is 78°, 73° and 66° when the γ -phase is formed on steel, α -alumina and γ -alumina substrate respectively.

5.2 Yttria partially-stabilized zirconia

Because of stable chemical and thermal properties, a low thermal conductivity and a relatively high coefficient of thermal expansion, yttria partially-stabilized (YPS) zirconia is now widely used as thermal barrier coating on turbine engine components in order to increase engine operating temperatures and concomitant efficiency (Bartlett & Maschio 1995). The plasma spray is an effective and relatively simple method for applying these coatings. A critical issue in YPS zirconia thermal barrier coatings is the control of yttria concentration to prevent the transformation from the tetragonal to monoclinic phase during thermal cycling. The distribution or segregation of yttria in a YPS zirconia splat depends on the interface morphology preferred during its solidification. A planar interface leads to a uniform distribution of yttria, which is particularly true when the solute trapping is large due to a high rate of solidification and a low diffusivity of the yttria in zirconia. A cellular or dendritic solidification, on the other hand, results in microsegregation (depletion) of yttria at the boundary of cells or dendrites, leading to the formation of monoclinic phase. In addition, the rapid solidification condition in plasma spray helps to generate a metastable, e.g., t' , phase that may have higher intrinsic toughness and is difficult to decompose into the equilibrium tetragonal and monoclinic phases.

Significant efforts have been made recently to develop better understanding of the microstructure and phase formation in YPS zirconia splats and coatings (Sampath *et al* 1999; Goswami *et al* 1999). It is found that, when a YPS zirconia coating is sprayed on a hot substrate, thin splats in the coating show columnar structure with uniform distribution of yttria. An epitaxial growth occurs when the two splats contact very well in the coating. However, for thicker splats in the coating produced on a cold substrate, nano-size particles made of monoclinic phase are observed with the spacing between the nano-particles ranging from 20 to 40 nm, as shown in figure 9 (Goswami *et al* 1999). The formation of such nanometer-size monoclinic phase particle indicates segregation of yttria during the columnar solidification. This is possible only if the solidification takes place with a cellular morphology, and as a result, the segregation occurs at the cell boundaries.

The model has also been employed to study the solidification characteristics of single splats of pure zirconia and yttria partially-stabilized zirconia (Wang G-X *et al* 2000b). YPS zirconia was treated as a diluted binary system with an equilibrium partition coefficient, $k_e = 2.1$, and the equilibrium liquidus slope, $m_L^0 = 2.9$ K/wt%. The steady-state, dendritic growth model was used to determine the range of the tip radius and therefore the spacing of the cells, which, according to Lu *et al* (1994), is approximately twice the tip radius under the rapid solidification conditions. Unfortunately, the model requires information on both the solid/liquid interface energy and the solute diffusivity of yttria in the melt, which are currently not known. After several attempts, it was found that the tip growth model would predict the tip radius and absolute stability velocity as shown in figure 10 if the diffusivity and Gibbs-Thomson constant are chosen as, $D_L = 5 \times 10^{-10}$ m²/s and $\Gamma = 10^{-8}$ Km



Figure 9. Nanometer nanocelmic particles within columnar grains of a zirconia-8wt% yttria coating plasma sprayed on a cold substrate (Goswami *et al* 1999)

respectively. Using such values, the tip radius is predicted to be in the range of 20 to 30 nm, giving a cell spacing of about 40 to 60 nm as observed in our experiments. The predicted absolute stability velocity is then about 0.3 m/s.

Wang G-X *et al* (2000b) used the planar interface model to characterize the rapid solidification of a zirconia splat. Figure 11 presents the calculated interface velocity as a

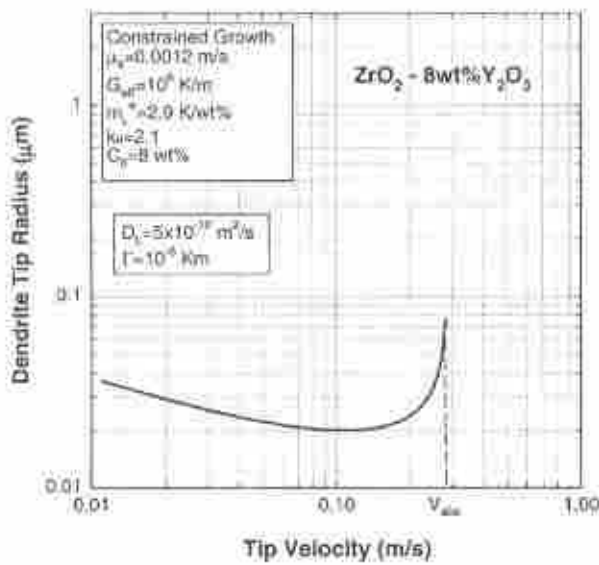


Figure 10. Model calculated tip radius as a function of the tip velocity for a PYS zirconia cell or dendrite when $\Gamma = 10^{-8}$ K/m and $D_L = 5 \times 10^{-10}$ m²/s (Wang G-X *et al* 2000b).

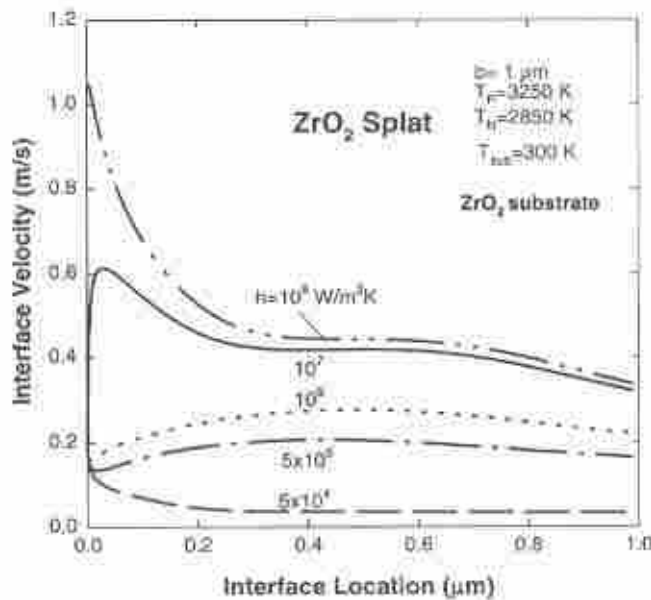


Figure 11. Interface velocity as a function of the interface location from the contact surface for a pure zirconia splat quenched on a zirconia substrate: effect of the thermal contact (Wang G-X *et al* 2000b).

function of the interface location when a 1 μm thick splat is quenched on a ZrO_2 substrate (which is used to simulate the previous deposit in the coating). The effect of the interfacial heat transfer coefficient is also shown in figure 11, and as expected, a higher value of h leads to a higher interface velocity. The interface velocity is smaller than 0.3 m/s when h is lower than $10^6 \text{ W/m}^2\text{K}$. It increases with h , but when h becomes larger than $10^7 \text{ W/m}^2\text{K}$, further increase in h results in only a minor increase in the interface velocity except during the early stages of solidification when the solidified layer thickness is small. This is because in the case of very high h , the thermal resistance to latent heat removal is controlled mainly by heat conduction through the solidified solid layer. Since the absolute stability velocity for YPS zirconia is about 0.3 m/s, it is expected that a stable planar interface exists for high values of h . When h is low, e.g., smaller or equal to $10^6 \text{ W/m}^2\text{K}$, the planar interface is not stable, and a cellular structure is expected. Such model predictions agree well with experimental observations. Columnar grains with planar interface solidification are observed in the splats or coatings sprayed on a hot substrate where good thermal contact is achieved between the splats. On the other hand, nano-sized monoclinic particles are formed in coatings sprayed on a cold substrate where thermal contact is poor (Goswami *et al* 1999).

One interesting issue relevant to the solidification morphology development is temperature distribution in the splat. It is well-known that a negative gradient of the melt temperature in front of the interface may develop in splat quenching, which may lead to the instability of the planar interface (Trivedi & Kurz 1986). Figure 12 shows the temperature distribution in a thin splat (0.5 μm) when good contact exists between the splat and the previous deposit, $h = 10^7 \text{ W/m}^2\text{K}$. An inspection of figure 12 shows that a positive temperature gradient exists in the liquid in front of the moving interface (where a kink appears in the temperature distribution) during the entire period of splat solidification. The existence of such positive temperature gradient indicates that the interface movement is under constraint of a positive temperature gradient, and the latent heat released at the

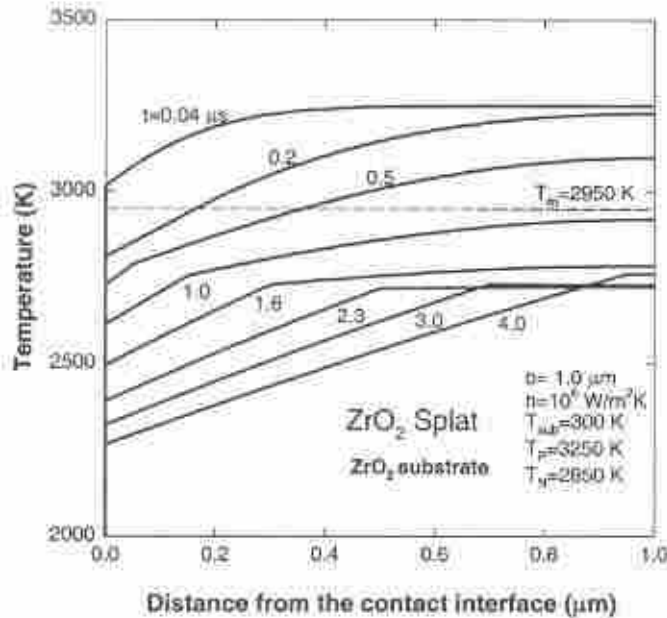


Figure 12. Temperature distributions at different time instants in a 1 μm thick ZrO_2 splat quenched on a ZrO_2 substrate with $h = 10^6 \text{ W/m}^2 \text{ K}$. Note that a positive temperature gradient exists in the melt all the time in front of the solid/liquid interface where a kink appears (Wang G-X *et al.* 2000b).

interface is carried away through the solidified solid, although there is a significant undercooling of the melt. This behaviour is quite different from that in the case of metals in which a large amount of latent heat is transferred into the undercooled melt (Wang G-X & Matthys 1991).

5.3 Mo and Mo-based alloys

Mo and Mo-based materials (e.g., Mo-C) have been employed for their good wear properties. It is also an interesting material for research in thermal spray. Columnar grains oriented perpendicular to the coating-substrate interface have been observed in Mo coatings (Moreau *et al.* 1992; Sampath & Herman 1996). The formation of this structure can be attributed to the columnar growth from the crystal nuclei nucleated at the interface between the molten lamella and the underlying molybdenum coating.

Robert *et al.* (1998b) have calculated the grain density in a single Mo splat sprayed on a steel substrate and compared their model predictions with their AFM measurements. A large discrepancy is reported between the theory and the measurements. Such discrepancies may partially be attributed to the uncertainty in the values of the solid/liquid interfacial energy and the contact angle between the crystalline Mo and the substrate. It should, however, be noted that the grain sizes measured by AFM from the topography of the splat top surface are much smaller than that observed by Sampath & Herman (1996) using transmission electron microscopy (TEM). One possible explanation to this variation is that the grains observed by AFM are not the real grains but the cell boundaries. Indeed, cellular solidification is possible in a sprayed Mo splat or coating since oxygen may be absorbed into the molten Mo droplets in flight. Indeed, TEM characterization does show the existence of various phases and cellular structures in Mo coatings. Efforts are being made to examine this issue both experimentally (Goswami 1999) and mathematically (Wang G-X *et al.* 2000c).

Recently, Jiang *et al.* (2000) have found extremely large size grains developed on the Mo splats sprayed on a high-temperature glass substrate with average grain sizes of about 5 μm

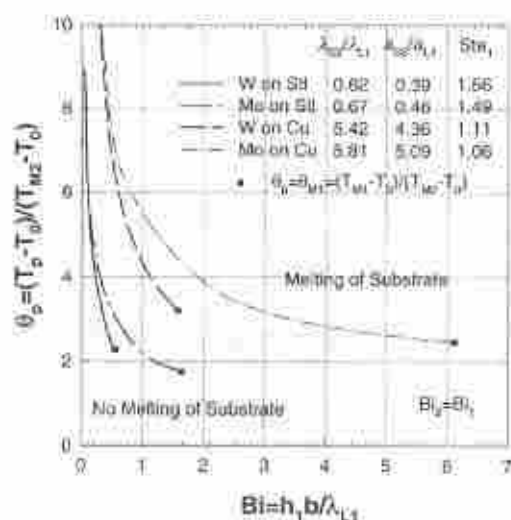


Figure 13. Operational map for the onset of substrate melting for an Mo splat sprayed on various substrate. Critical conditions for various deposit/substrate combinations (Wang S-P *et al.* 1999).

diameter, even larger than the thickness of the splat. (The average thickness of the splats is about 0.5 to 1.0 μm .) It is speculated that in this case, the melt is significantly undercooled and only few nuclei are formed either within the bulk melt or on the substrate surface with nuclei being far away from each other. The nuclei then grow quickly to the top surface before they can impinge onto each other. After this, solidification occurs laterally along the surface of the substrate and stops when grains touch all neighbouring grains (Wang G-X *et al.* 2000c). The grain growth model described in § 3.3 cannot be applied to such solidification patterns and a new model is needed to take into account the multi-dimensional effect of the grain growth.

Due to high melting point and large latent heat, significant substrate melting is observed at the Mo splat/substrate interface (Jiang *et al.* 1999; Goswami 1999, unpublished data). Theoretical investigation of substrate melting has been carried out by Wang S-P *et al.* (1998, 1999) and operational maps such as the one shown in figure 13 have been developed. The map is divided into two regions, melting and non-melting of the substrate, and the curves in the figure are the loci of the process parameter combinations that correspond to the onset of substrate melting. If the process parameters belong to the upper region (larger splat/substrate temperature difference or larger Biot number), the substrate melting occurs and vice-versa. For high melting point materials such as Mo, a minimum exists at which the substrate melts even if the initial melt temperature is the melting temperature, i.e., no superheat. This requires a large Biot number, i.e., a large interface heat transfer coefficient, or a thick deposit.

The model can also predict the velocities of substrate melting and resolidification as shown in figure 14 for one set of parameters. Clearly, the interfacial heat transfer coefficient controls both substrate melting and resolidification velocities. In general, substrate resolidification velocity is smaller than melting speed.

6. Concluding remarks

A brief review of the recent progress made in the area of theoretical modelling and experiments for microstructure development in thermally sprayed single splats and

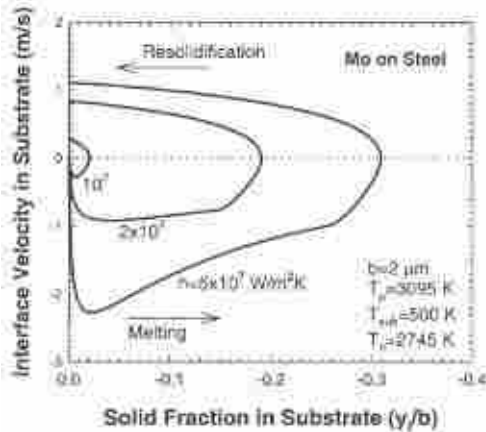


Figure 14. Substrate melting and resolidification velocity for a thin Mo splat sprayed on a steel substrate under three interfacial heat transfer coefficients (Wang S-P et al 1999).

coatings have been presented. A model has been developed that incorporates the basic physical principles of various kinetic processes in thermal sprays. The physical phenomena include heat and mass transfer, melt undercooling, selective nucleation of stable and metastable phases, non-equilibrium kinetics of crystalline growth, solidification morphology and transition, thermal resistance at the splat/substrate and splat/splat interfaces, and substrate melting and resolidification. The model has been used to characterize the rapid solidification of a single splat in plasma-sprayed coatings. Both metallic and ceramic materials have been studied, including molybdenum, alumina, and partially yttria-stabilized zirconia. Model predictions together with experimental observations and measurements provide special insights into microstructure development in plasma-sprayed coatings. Good qualitative agreement between the theory and experiments has been found in many cases.

The model, however, involves several various assumptions and approximations that restrict the application of the model. Many of these approximations are not realistic and further work is needed to relax them and develop more accurate models. In particular, the model is based on one-dimensional heat and mass transfer conditions, and does not include the effect of initial melt spreading and droplet deformation. A one-dimensional geometry cannot effectively deal with crystalline nucleation which is basically a three-dimensional phenomenon. This also excludes an accurate treatment of equiaxed solidification such as in the case of Mo on a glass substrate (Jiang et al 2000). Efforts are currently being made to improve the model by removing these assumptions and approximations and to apply the model to other material systems.

References

- Aziz M J 1982 Model for solute redistribution during rapid solidification. *J. Appl. Phys.* 53: 1158–1168
- Baker J C, Cahn J W 1971 Thermodynamics of solidification. In *Solidification* (Metals Park, OH: Am. Soc. Metals) pp 23–58
- Burlett A H, Maschio R D 1995 Failure mechanisms of a zirconia-8 wt% yttria thermal barrier coating. *J. Am. Ceram. Soc.* 78: 1018–1024
- Battle T P 1992 Mathematical modeling of solute segregation in solidifying materials. *Int. Mater. Rev.* 37: 249–270
- Beckermann C, Wang C Y 1995 Multiphase-scale modeling of alloy solidification. *Annu. Rev. Heat Transfer* 6: 115–198
- Boettinger W J, Coriell S R 1986 Microstructure formation in rapidly solidified alloys. In *Science and technology of the undercooled melt* (eds) P R Sahm, H Jones, C M Adam (Martinus Nijhoff) pp 81–109
- Carrard M, Gremaud M, Zimmermann M, Kurz W 1992 About the banded structure in rapidly solidified dendritic and eutectic alloys. *Acta Metall. Mater.* 40: 983–996
- Clyne T W 1982 Numerical modeling of directional solidification of metallic alloys. *Metal Sci.* 16: 441–450
- Clyne T W 1984 Numerical treatment of rapid solidification. *Metal. Trans.* B15: 369–381
- Feuerbacher B 1989 Phase formation in metastable solidification of metals. *Mater. Sci. Rep.* 4: 1–40
- Flood S C, Hunt J D 1987 Columnar and equiaxed growth. I. A model of a columnar front with a temperature dependent velocity. *J. Crystal Growth* 82: 543–551
- Gansert R V 1996 *Plasma-spray processing of alumina-based free-forms using water-stabilized plasma*. Ph D thesis, State University of New York at Stony Brook, Stony Brook
- Giovanola B, Kurz W 1990 Modeling of microsegregation under rapid solidification conditions. *Metal. Trans.* A21: 260–263
- Goswami R, Wang G-X, Sampath S, Herman H 1999 Synthesis of zirconia-8wt.% yttria nanocomposites by thermal spray. 1999 *TMS Annual Meeting*, San Diego, CA (Warrendale, PA: TMS)
- Granasy L, Ludwig A 1992 Impact of casting conditions on the dendritic solidification in single roller quenching methods (simulation). In *Melt-spinning and strip casting: Research and implementation* (ed.) E F Matthys (Warrendale, PA: TMS), pp 53–68
- Jacobson I. A, McKittrick J 1994 Rapid solidification processing. *Mater. Sci. Eng.* R11: 355–408
- Jiang X Y, Sampath S, Matejcek J 1999 Substrate temperature effects on splat formation, microstructure development and properties of plasma sprayed coatings. Part II: Case study for molybdenum. *Mater. Sci. Eng.* A272: 189–198
- Jiang X Y, Sampath S, Herman H 2000 Grain morphology of molybdenum splats plasma-sprayed on glass substrates. *Mater. Sci. Eng. A* (submitted)
- Karma A, Sarkissian A 1993 Interface dynamics and banding in rapid solidification. *Phys. Rev.* 47: 513–533
- Kim S G, Shin S H, Suzuki T, Umeda T 1994 Numerical analysis of the rapid solidification of gas-atomized Al-8 wt pct Fe droplets. *Metal. Mater. Trans.* A25: 2815–2826
- Kurz W, Fisher D J 1989 *Fundamentals of solidification* 3rd edn (Trans. Tech. Publ.)
- Levi C G 1988 The evolution of microcrystalline structures in supercooled metal powders. *Metal. Trans.* A19: 699–708
- Levi C G, Mehrabian R 1982 Heat flow during rapid solidification of undercooled metal droplets. *Metal. Trans.* A13: 221–234
- Lu S Z, Hunt J D, Gilgien P, Kurz W 1994 Cellular and dendritic growth in rapidly solidified Al-Fe and Al-Cu alloys. *Acta Metall. Mater.* 42: 1653–1660

- McPherson R 1980. On the formation of thermally sprayed alumina coatings. *J. Mater. Sci.* 15: 3141–3149
- Moreau C, Lamontagne M, Cielo P 1992 Influence of the coating thickness on the cooling rates of plasma-sprayed particles impinging on a substrate. *Surf. Coating Techn.* 53: 107–114
- Mostaghimi J, Pasandideh-Fard M, Azar R G, Chandra S 1999 Modeling of the formation of thermal spray coatings. Presented at the Mater. Res. Soc. Fall Meeting, Boston, MA
- Rappaz M 1989 Modelling of microstructure formation in solidification processes. *Int. Mater. Rev.* 34: 93–123
- Robert C, Denoirjean A, Vardelle A, Wang G-X, Sampath S 1998a Nucleation and phase selection in plasma-sprayed Al₂O₃: Modeling and experiments. *Proc. 15th Int. Thermal Spray Conference*, Nice, France, pp 407–412
- Robert C, Vardelle A, Wang G-X, Jiang X, Sampath S 1998b Microstructure development during plasma spraying of molybdenum, Part I: Splat solidification. *Proc. 15th Int. Thermal Spray Conference*, Nice, France, pp 729–734
- Sampath S, Herman H 1996 Rapid solidification and microstructure development during plasma spraying. *J. Thermal Spray Tech.* 5: 445–456
- Sampath S, Neiser R A, Herman H, Kirkland J P, Elam W T 1993 A structural investigation of a plasma sprayed Ni-Cr based alloy coating. *J. Mater. Res.* 8: 78–86
- Sampath S, Jiang X Y, Matejcek J, Leger A C, Vardelle A 1999 Substrate temperature effects on splat formation, microstructure development and properties of plasma sprayed coatings, Part I: Case study for partially stabilized zirconia. *Mater. Sci. Eng.* A272: 181–188
- Trapaga G, Szekely J 1991 Mathematical modeling of the isothermal impingement of liquid droplets in spraying processes. *Metall. Trans. B* 22: 901–914
- Trivedi R, Kurz W 1986 Morphological stability of a planar interface under rapid solidification conditions. *Acta Metall.* 34: 1663–1670
- Trivedi R, Kurz W 1994 Dendritic growth. *Int. Mater. Rev.* 39: 49–74
- Vardelle A, Robert C, Wang G-X, Sampath S 1997 Analysis of nucleation, phase selection and rapid solidification of an alumina splat. In *Thermal spray: A united forum for scientific and technological advances* (ed.) CC Berndt (Materials Park, OH: ASM Int.) pp 635–643
- Wang G-X, Matthys E F 1991 Modeling of heat transfer and solidification during splat cooling: Effect of splat thickness and splat/substrate thermal contact. *Int. J. Rapid Solidification* 6: 141–174
- Wang G-X, Matthys E F 1992 Numerical modeling of phase change and heat transfer during rapid solidification processes: Use of control volume integral with element subdivision. *Int. J. Heat Mass Transfer* 35: 141–153
- Wang G-X, Matthys E F 1993 Modeling of rapid planar solidification of a binary alloy. In *Heat and mass transfer in materials processing and manufacturing* (New York: ASME) vol. HTD-261, pp 35–44
- Wang G-X, Matthys E F 1996a Modeling of surface melting and resolidification for pure metals and binary alloys: Effect of non-equilibrium kinetics. *J. Heat Transfer* 118: 944–951
- Wang G-X, Matthys E F 1996b Experimental investigation of interfacial thermal resistance for molten metal solidification on a substrate. *J. Heat Transfer* 118: 157–163
- Wang G-X, Matthys E F 1996c On the heat transfer at the interface between a solidifying metal and a solid substrate. In *Melt-spinning, strip casting, and slab casting* (eds) E F Matthys, W G Truckner (Warrendale, PA: TMS) pp 205–236
- Wang G-X, Prasad V 2000 Rapid solidification: Fundamentals and modeling. *Annu. Rev. Heat Transfer* 11: 207–305
- Wang G-X, Prasad V, Sampath S, Herman H 1998 A mathematical model for microsegregation in rapidly solidified alloys. In *Modeling casting, welding advanced solidification processes - VIII*, (eds) B G Thomas, C Beckermann (Warrendale, PA: TMS) pp 219–226
- Wang G-X, Prasad V, Sampath S 2000a An integrated model for dendrite and planar interface growth and morphology transition in rapid solidification. *Metall. Mater. Trans.* A31: 735–746

- Wang G-X, Goswami R, Sampath S, Prasad V 2000b Heat transfer and solidification analysis of splat formation in plasma-sprayed zirconia-yttria thermal barrier coatings. *4th ISHMT-ASME Heat Transfer Conference* (New Delhi: Tata McGraw-Hill) pp 1135-1140
- Wang G-X, Jiang X Y, Sampath S 2000c Grain structure development in plasma sprayed coatings: Experiment and modeling. In *Surface engineering in materials science 1* (eds) S Seal et al (Warrendale, PA: TMS) pp 197-209
- Wang S-P, Wang G-X, Mathys E F 1998 Melting and resolidification of a substrate in contact with a molten metal: Operational maps. *Int. J. Heat Mass Transfer* 41: 1177-1188
- Wang S.P, Wang G-X, Mathys E.F 1999 Deposition of a molten layer of high melting point material: Substrate melting and resolidification. *Mater. Sci. Eng. A262*: 25-32
- Zhang H 1999 Theoretical analysis of spreading and solidification of molten droplet during thermal spray deposition. *Int. J. Heat Mass Transfer* 42: 2499-2508